Biochimica et Biophysica Acta 1818 (2012) 1427–1434

Contents lists available at SciVerse ScienceDirect

Biochimica et Biophysica Acta

journal homepage: www.elsevier.com/locate/bbamem

Gross morphological changes in thylakoid membrane structure are associated with photosystem I deletion in *Synechocystis* sp. PCC 6803

Allison M.L. van de Meene [a,*,1], William P. Sharp [a], Jennifer H. McDaniel [a], Heiner Friedrich [b,2], Wim F.J. Vermaas [a], Robert W. Roberson [a]

[a] School of Life Sciences, Arizona State University, Tempe, AZ 85287-4501, USA
[b] Center for Solid State Sciences, Arizona State University, Tempe, AZ 85287-4501, USA

ARTICLE INFO

Article history:
Received 24 October 2011
Received in revised form 20 January 2012
Accepted 20 January 2012
Available online 27 January 2012

Keywords:
Electron tomography
Photosynthesis
Thylakoid membrane
Photosystem I
Photosystem II
Phycobilisome

ABSTRACT

Cells of *Synechocystis* sp. PCC 6803 lacking photosystem I (PSI-less) and containing only photosystem II (PSII) or lacking both photosystems I and II (PSI/PSII-less) were compared to wild type (WT) cells to investigate the role of the photosystems in the architecture, structure, and number of thylakoid membranes. All cells were grown at 0.5 μmol photons m^{-2} s^{-1}. The lumen of the thylakoid membranes of the WT cells grown at this low light intensity were inflated compared to cells grown at higher light intensity. Tubular as well as sheet-like thylakoid membranes were found in the PSI-less strain at all stages of development with organized regular arrays of phycobilisomes on the surface of the thylakoid membranes. Tubular structures were also found in the PSI/PSII-less strain, but these were smaller in diameter to those found in the PSI-less strain with what appeared to be a different internal structure and were less common. There were fewer and smaller thylakoid membrane sheets in the double mutant and the phycobilisomes were found on the surface in more disordered arrays. These differences in thylakoid membrane structure most likely reflect the altered composition of photosynthetic particles and distribution of other integral membrane proteins and their interaction with the lipid bilayer. These results suggest an important role for the presence of PSII in the formation of the highly ordered tubular structures.

1. Introduction

Oxygenic photosynthesis is undertaken by both plants and cyanobacteria. These organisms convert light energy to chemical energy in the photolysis of water, releasing electrons into an electron transfer chain generating chemical potential energy, and liberating oxygen. The site of photosynthesis in these organisms is a specialized membrane system called the thylakoid membrane. Macromolecular protein complexes involved in photosynthesis are embedded within thylakoid membranes and are also found as peripheral antenna in cyanobacteria and algae.

The structural basis of photosynthesis in both cyanobacteria and higher plants is understood from spectroscopic studies and X-ray crystallography of photosynthetic complexes [1,2]. In higher plants, the chlorophyll *b* containing light harvesting complex (LHC), which is associated with photosystem II (PSII), is implicated in the formation of thylakoid stacks, also called grana membranes, by electrostatic forces [3]. In cyanobacteria, there are no LHCs, but rather phycobilisomes that that are extrinsic to the cytoplasmic side of the thylakoids and act as antenna complexes for light capture. The presence of phycobilisomes prevents the possibility of grana-like stacking of the thylakoid membranes. The role of the photosystems themselves in determining the structure of thylakoid membranes is not clear. To study the role of PSII on thylakoid architecture we investigated a mutant of *Synechocystis* sp. PCC 6803 lacking a functional photosystem I (PSI) complex [4] leaving only PSII present and a mutant lacking both PSI and PSII [5]. A previous study [22] reported on the ultrastructural and biochemical characteristics of a mutant lacking only PSII.

Cyanobacteria are ideal organisms to investigate questions regarding processes and structures associated with oxygenic photosynthesis. In particular, *Synechocystis* sp. PCC 6803 is a useful model cyanobacterium as the genome has been sequenced [6], genetic manipulations are straightforward [7], and this organism can be grown with an external carbon source allowing the deletion of photosynthetic components. Protocols for measurements of photosynthesis have been developed and this organism is amenable to cryofixation techniques for ultrastructural analysis [8–10].

Abbreviations: PSI, Photosystem I; PSII, Photosystem II; FF, freeze fracture; EF, endoplasmic face; PF, protoplasmic face; LHC, light harvesting complex

* Corresponding author at: School of Life Sciences, P.O. Box 874501, Arizona State University, Tempe, AZ 85287-4501, USA. Tel.: +1 480 965 8618; fax: +1 480 965 6899.
E-mail address: Robert.Roberson@asu.edu (A.M.L. van de Meene).
[1] Present address: Centre for Bioimaging, Rothamsted Research, Harpenden, Herts, AL5 2JQ, UK.
[2] Present address: Laboratory of Materials and Interface Chemistry, Department of Chemical Engineering and Chemistry, Eindhoven University of Technology, Den Dolech 2 5612 AZ Eindhoven, The Netherlands.

0005-2736/$ – see front matter © 2012 Elsevier B.V. All rights reserved.
doi:10.1016/j.bbamem.2012.01.019

The PSI-less mutant investigated lacks the *psaA* and *psaB* genes that encode the core reaction center proteins necessary for the assembly of the PSI complex. These deletions allow detailed investigations into PSII [4].

The PSI/PSII-less mutant lacks the PSI core genes psaA and psaB, as well as the two copies of the psbD gene and psbC [5]. The psbD genes encode the PSII reaction center protein D2 that binds essential redox co-factors necessary for photosynthetic electron transfer. The last gene, psbC, encodes the CP43 protein. The PSI-less mutant only grows at low light intensities of 0.5 μmol photons m^{-2} s^{-1} or less presumably due to the reduction of the plastoquinone pool at higher light intensities. Both the PSI-less and the PSI-less/PSII-less strains require glucose as a fixed-carbon source.

The organization and structure of the thylakoids in these mutants and in wild type (WT) cells grown at low light intensities was determined using transmission electron microscopy and electron tomography. The number of thylakoid membranes and the volume of the thylakoid membranes and the enclosed lumen were determined from the electron micrographs using stereological methods for statistical analysis. The distributions, sizes and numbers of intermembrane particles were investigated using freeze fracture/freeze etch analysis. PSII-less cells were not investigated as Nilsson and coworkers [22] investigated such a mutant previously using FF and TEM techniques.

The differences observed in this study can be correlated to biochemical and physiological properties that have previously been described in these mutants and give some insight into how the functional photosystems are involved in thylakoid structure.

2. Materials and methods

2.1. Cell culture

Synechocystis sp. PCC 6803 cells were maintained on sterile agar plates made with BG-11 medium [11] with 10 mM TES-NaOH (pH 8.0), 1.5% agar, 10 mM glucose and 0.3% sodium thiosulfate added. For the PSI-less mutant [4] 25 μg/ml chloramphenicol was added to the agar plate. For the PSI/PSII-less mutant [5] 25 μg/ml chloramphenicol, 10 μg/ml erythromycin, and 25 μg/ml spectinomycin were added. For liquid culture, the cells were grown in 50 ml of BG-11 medium containing 5 mM TES-NaOH (pH 8.0) with the relevant antibiotics and 5 mM glucose in 100 ml Erlenmeyer flasks on an orbital shaker at 140 rpm. All cell types, including WT, were grown continuously at a light intensity of 0.5 μmol photons m^{-2} s^{-1} at a constant temperature of 30 °C.

2.2. Transmission electron microscopy

Cells in the logarithmic growth phase were spun in 50 ml centrifuge tubes at 1200 rpm in a medical centrifuge for 10 min to form a pellet. Approximately 20 μl aliquots of the cell pellet were placed onto a Formvar-coated copper grid, which was then placed between the flat sides of two B-type brass planchets (Ted Pella Inc., Redding, CA). The copper grid is used as a spacer creating a thin layer of cells that allowed for a higher yield of well frozen cells. The cells were high pressure frozen using a Bal-Tec HPM 010 High Pressure Freezing Machine (Bal-Tec Products, Middlebury, CT). Following cryofixation, the samples were freeze-substituted at −85 °C in 1% glutaraldehyde (Electron Microscopy Sciences, Washington, PA) and 1% tannic acid in HPLC-grade anhydrous acetone for 72 h. The samples were then rinsed in three changes of anhydrous acetone at −85 °C before being placed in a 1% OsO_4 solution in acetone and slowly warmed to room temperature over a six-hour period. The cells were then rinsed in acetone and slowly infiltrated with and polymerized in Spurr's resin [12]. Embedded cells were cut into serial 70 nm thick sections with an Ultracut R Microtome (Leica, Vienna, Austria) and collected on Formvar-coated copper slot grids. Sections were post-stained with 2% uranyl acetate in 50% ethanol for 5 min followed by 5 min with Reynolds' lead citrate [13]. The grids were carbon-coated and viewed at 80 kV using an FEI CM12S transmission electron microscope (FEI Company, Mahwah, NJ). At least 100 cell images were taken, at random, of each strain investigated. Images of these sections were captured digitally with a 1 K Multiscan CCD Camera (Gatan Inc., Pleasanton, CA) using Digital Micrograph software (Gatan).

The number of thylakoid membrane sheets per cell was counted for 100 random cell images of each strain to determine whether there was a difference in the average numbers of thylakoid membrane sheets per cell between the strains. The relative volumes of the lumen of these thylakoid membrane sheets were compared to the cytoplasmic volume using stereological methods [14,15].

2.3. Electron tomography

The embedded cells were prepared for electron tomography as described in [10]. Thick sections (100–200 nm) were cut with an Ultracut R microtome (Leica, Vienna, Austria) and collected on grids post-stained as described above. Fiducial markers were applied randomly to each surface of the sections in the form of 10 nm colloidal gold particles (Sigma, St. Louis, MO). Dual-axis electron tomograms were collected using a Tecnai F20 intermediate-voltage electron microscope (IVEM) (FEI Company, Hillsboro, OR) at 200 kV at the Center for Solid State Sciences (Arizona State University, AZ). Tomography data sets were obtained from selected cells by acquiring consecutive tilt views every 1° from −60° to +60° on a Gatan 1 K×1 K CCD camera. Tilt-series acquisition was carried out automatically at a nominal defocus of 0.8 μm by the tomography plugin for the ESVision data acquisition software (Emispec Inc., now FEI Company). For the collection of the tomographic tilt-series an in-house built high-tilt sample holder was used [16]. The datasets were subsequently aligned, reconstructed and visualized in IMOD [17–19]. A total of nine dual-axis tomograms, three of each cell type, were reconstructed and analyzed.

Tomographic figures selected in this paper represent cross sections through the complete tomographic reconstructions. The corresponding movie supplements display sequential sections through the reconstructed volume, i.e., moving from the front to the back side of the reconstruction. Movies were generated using QuickTime Pro (Apple Computers, Cupertino, CA). Tomography data sets were obtained from selected cells by digitally collecting consecutive tilt views every 1° from −60° to +60°. The size of the pixels in the tomograms was 1.1 nm giving a 4–5 nm resolution in the X- and Y-axes and 6–7 nm in the Z-axis due to the point spread function of the microscope. A total of nine dual-axis tomograms, three of each cell type, were reconstructed.

2.4. Freeze fracture

For freeze fracture, cells were prepared for high pressure cryofixation as described above. However, instead of the B-type planchets, solid gold or brass edge-to-edge planchets (3 mm×0.8 mm) (Baltec RMC distributed by Boeckler Instruments Inc., Tucson, AZ) were used. The cells were placed directly on the flat surface of the planchet prior to freezing and no copper slot grid was used as cells needed to stay on the surface of the planchet for fracturing. Two of the planchets were appressed together for freezing, which allowed a thin layer of cells to be frozen without reducing the size or conductivity of the planchets. These specimen carriers could fit into both the specimen holder for the high-pressure freezer and the Balzers 400D Freeze-Etch Unit (Balzers Corp., Nashua, NH) where the cells were fractured as the two planchets were separated. If required, the knife in the chamber could be used to further fracture the material. Following fracturing, the cells were etched at −110 °C for 5 min at a pressure of 10^{-6} mbar. The specimen was then shadowed with platinum from a 45° angle and the replica was backed with carbon applied from directly above [20]. To clean the replicas, the planchets, cells

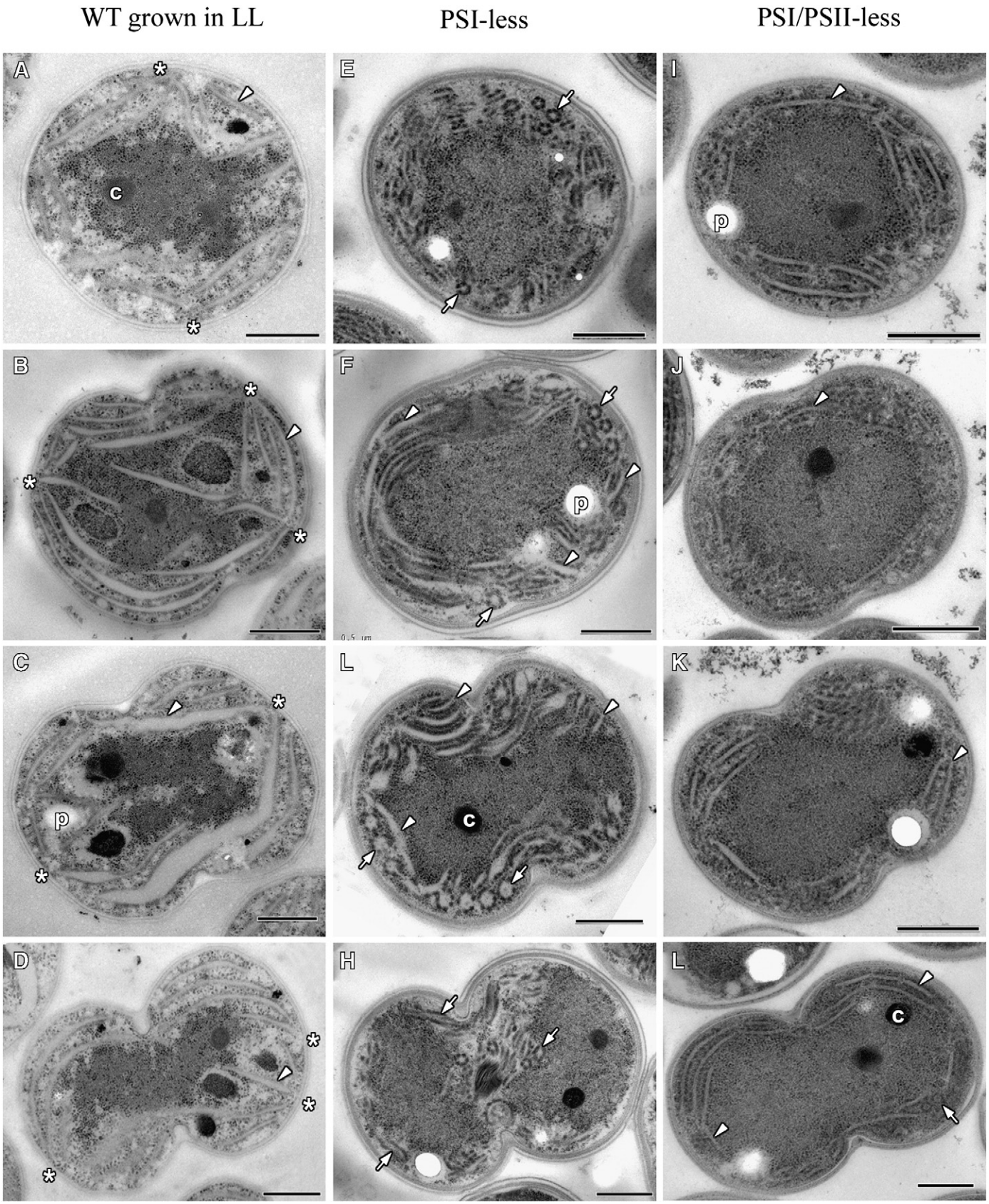

Fig. 1. TEM images of Synechocystis sp. PCC 6803 wild type cells grown at 0.5 mol photons m^{-2} s^{-1} (A–D), PSI-less cells (E–H), and PSI/PSII-less cells (I–L) both grown under the same conditions as the wild type cells. The thylakoid membrane pairs (white arrowheads) form layers around the periphery of the cell in all three cell types converging adjacent to the cytoplasmic membrane at various points around the cell (asterisks). Carboxysomes (c) and polyhydroxyalkanoate granules (p) are present in the cells. The PSI-less cells (E–H) have tubes of thylakoid membranes that are surrounded by electron opaque phycobilisomes and can be seen in both cross section as circles and longitudinal section as tubes (white arrows). Similar tubes are seen in the PSI/PSII-less cells. Scale Bars = 200 nm.

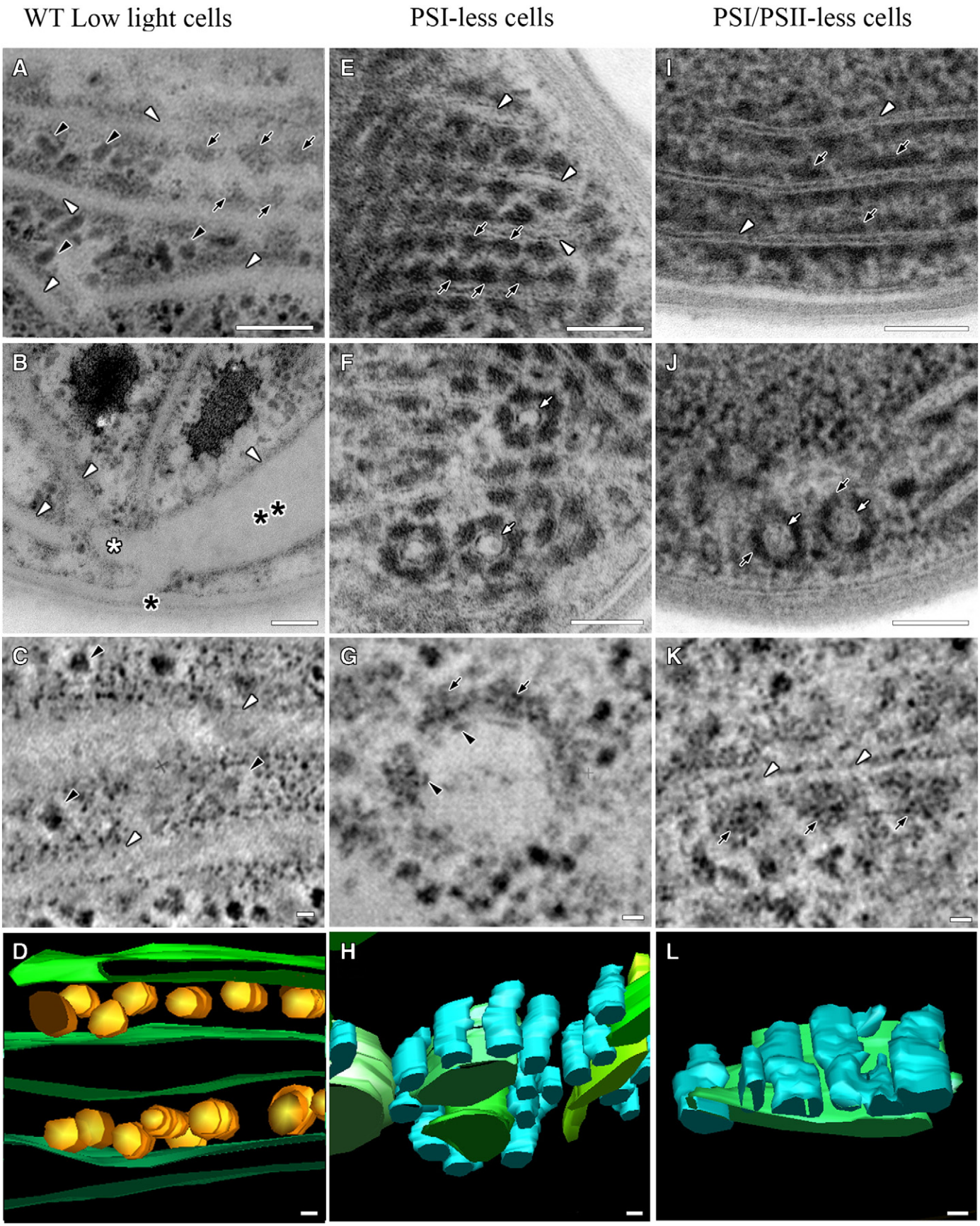
WT Low light cells
PSI-less cells
PSI/PSII-less cells
A
E
I
B
F
J
C
G
K
D
H
L

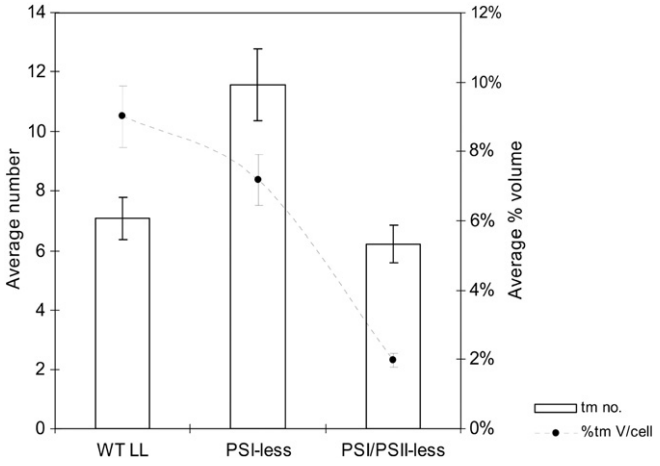

Fig. 3. Average number of thylakoid membrane pairs and percentage thylakoid volume per cell per strain. The PSI-less mutant has more thylakoid membrane pairs per cell but the volume of the PSI-less and WT cells are not significantly different. The PSI /PSII-less cells have fewer thylakoid membrane pairs than the PSI-less mutant but similar number to the WT LL grown cells. The volume taken up by the thylakoid membranes in this mutant was significantly lower.

and replicas were initially placed in 15% methanol for 10 min, followed by 30 min in a 1:1 solution of 15% methanol and sodium hypochlorite before being placed in 100% sodium hypochlorite overnight at room temperature. The next day the planchets and replicas were rinsed three times in double distilled H_2O before the replica only was placed in 70% sulfuric acid for 5 h at 60 °C. The replicas were then rinsed again in double distilled H_2O before being placed on Formvar-coated mesh grids. The replicas were viewed at 80 kV using an FEI CM12S transmission electron microscope (FEI Co., Mahwah, NJ). The sizes of the particles on the surfaces of the thylakoid membranes were determined directly from the electron micrographs using the Metamorph Imaging System (Molecular Devices, Sunnyvale, CA).

3. Results

3.1. Thylakoid membrane organization and number

The thylakoid membranes were significantly different in all of the three strains of *Synechocystis* sp. PCC 6803 investigated (Figs. 1 & 2). The central region of cytoplasm within the thylakoid membranes contained the central cytoplasmic space with carboxysomes and was sometimes traversed by thylakoid membranes and other structures. Polyhydroxyalkanoate granules were found mostly around the periphery of the cells (Fig. 1).

Like cells grown at higher light intensities [8,10], the thylakoid membrane pairs of WT cells grown 0.5 μmol photons m^{-2} s^{-1} (Fig. 1A–D) formed stacks of parallel sheets that converged at points adjacent to the cytoplasmic membrane. In 15 cells out of 207 examined (7%) there were points of convergence where there appeared to be fusion between the cytoplasmic membrane and the thylakoid membranes, creating continuity of the periplasmic space and thylakoid lumen (Fig. 2B).

In the low light grown WT cells, the number of thylakoid membrane pairs in a stack ranged from 1–8 compared to 3–10 in cells grown at higher light [10]. However, in the low light grown cells, each thylakoid membrane pair enclosed what appeared to be an inflated thylakoid lumen that measured from approximately 10 nm in width up to almost 300 nm in some cells (Fig. 1A–D). The thylakoid membrane sheets were on average 30–120 nm apart and glycogen granules were packed between them (Fig. 2A, C–D, Supp. 1A, 1B). Phycobilisomes (Fig. 2A) were found more commonly on thylakoid membranes towards the outside of the cell than towards the inside.

In the PSI-less mutant (Fig. 1E–H), the thylakoid membranes formed stacks of 1–10 thylakoid membrane pairs. However, rather than always forming sheets (Fig. 2E) that enclosed the thylakoid lumen, these thylakoid membranes formed tubes around a lumen (Figs. 1E–H, 2F–H, Supp. 2A, 2B). These tubes were observed in 74% (129 out of 175) of PSI-less cells examined often followed through a number of 70 nm serial thin sections and were distinct from the thylakoid centers observed in WT cells grown in high light [10,21] as there was no internal structure observed in the PSI-less tubes and the diameter was variable. Phycobilisomes were prominent in this mutant along the thylakoid sheets and around the thylakoid tubes (Fig. 2E–H, Supp. 2). Glycogen granules were less prominent. At high magnification, structures could be seen directly beneath the phycobilisomes possibly extending into the lumen (Fig. 2G).

In the PSI/PSII-less mutant (Figs. 1I–L, 2I–L, Supp. 3A, 3B), thylakoid membrane sheets were also present around the periphery of the cell but were not as extensive and appeared to be reduced concentric sheets that did not form as many layers. However, the number of thylakoid membrane pairs per cell was similar to WT but fewer than the PSI-less mutant. The lumen was 5–8 nm in diameter in this strain, similar to WT cells grown at 50 μmol photons m^{-2} s^{-1} [10]. There were cylindrical structures (Figs. 1L, 2J) that appeared to be a cross between the tubes of the PSI-less mutant and the thylakoid centers of WT cells as there seemed to be some internal structure. These were not as common as the tubes in the PSI-less mutant but were still found in 18% (18 out of 100) of cells observed. In 70 nm thin sections, there appeared to be amorphous material of the same electron density consistent with that of the phycobilisomes observed in the PSI-less mutant over the surface of the thylakoid membranes and the tubes (Fig. 2I, J). In electron tomograms, it was more evident that these structures were hemispherical phycobilisomes that were not laid out in regular arrays (Fig. 2K, L). Otherwise this mutant was remarkably similar in appearance to WT cells grown under high light conditions.

An interesting variation among the three strains studied were the number of thylakoid sheets and the volume of the lumen enclosed within these sheets (Fig. 3). The number of thylakoid membrane sheets per cell was higher in the PSI-less mutant (average of 12) compared to the WT cells grown in low light (average of 7), although the overall volume of the lumen was greater in the WT cells (9% in WT cells and 7% in PSI-less cells). The PSI/PSII-less mutant had fewer thylakoid membrane sheets per cell (average of 6), which enclosed a smaller volume of lumen compared to the other two strains (2%).

3.2. Integral membrane protein distribution on thylakoid membranes

Freeze fracturing of the surface of the thylakoid membranes of the low light grown wild type cells (Fig. 4A, B) revealed the presence of

Fig. 2. TEM images (A–B, E–F, I–J), electron tomography images (C, G, K) and electron tomography models (D, H, L) of the thylakoid membranes of wild type cells grown at 0.5 mol photons m^{-2} s^{-1} (A–D), PSI-less cells (E–H), and PSI/PSII-less cells (I–L). In the 0.5 mol photons m^{-2} s^{-1} (A–D), the thylakoid membrane pairs (white arrowheads) enclose inflated lumen. Glycogen granules are apparent between the thylakoid pairs (black arrowheads). At a convergence site (asterisk), the inflated lumen (double black asterisk) is continuous with the periplasmic space (black asterisk). From electron tomography, location and size of the glycogen granules becomes more apparent and phycobilisomes were more difficult to observe. In the model the thylakoid membrane pairs (green) and glycogen granules (orange) are shown. In the PSI-less cells (E–H), numerous phycobilisomes (black arrows) are present on the surface of the thylakoid membranes and tubes (white arrowheads and arrows respectively) (E–G). Directly beneath the phycobilisomes, electron opaque structures (black arrowheads) project slightly into the lumen when observed in a 5 nm electron tomograph (G). The tomographic model shows two thylakoid membrane tubes and portions of thylakoid membrane sheets (green) with rows of phycobilisomes (blue) on the surface. In the PSI/PSII-less cells (I-L), phycobilisomes (black arrows) are present on the surface of the thylakoid membrane sheets (white arrowheads) (I, K). In these cells, there also appear to be tubes with phycobilisomes on the surface (J), similar to the tubes of thylakoid membranes in the PSI-less cell (white arrows). In the model the phycobilisomes (blue) form more disordered arrays on the surface of the thylakoid membrane sheet (green). Scale bars = 100 nm (A, B, E, F, I, J) and 20 nm (C, D, G, H, K, L).

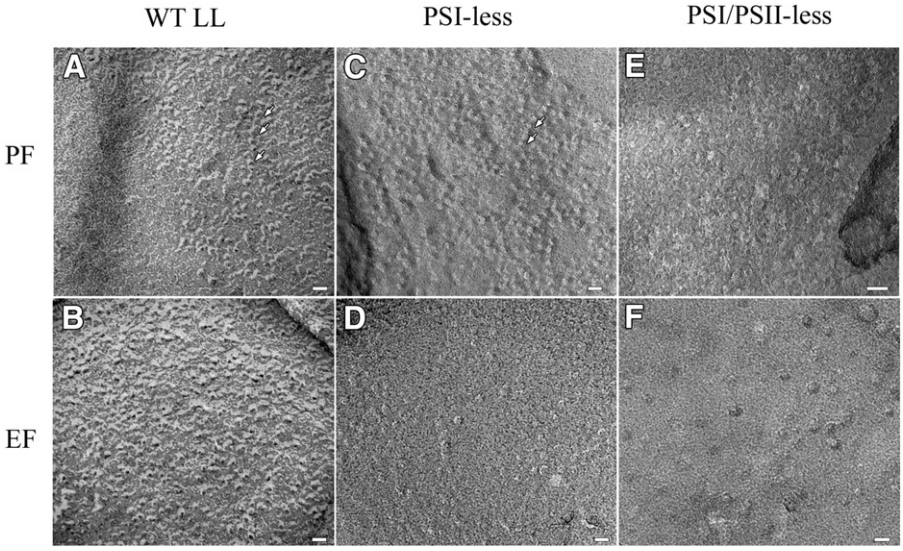

Fig. 4. Freeze fracture images of the PFs (A, C, E) and EFs (B, D, F) of the low light grown wild type cells (A–B), PSI-less cells (C–D) and PSI/PSII-less cells (E–F). There is a higher density of particles on the P-faces of all three species than on the E-faces. The P-faces also show rows of particles on the wild type low light grown cells and the PSI-less cells (white arrows).

3997 particles/μm^2 on the protoplasmic face (PF) and 902 particles/μm^2 on the endoplasmic face (EF). PF particles were 6–12 nm in diameter. The EF particles were 4–9 nm in diameter. Some PF particles formed rows on the thylakoid membranes (Fig. 4A).

In the PSI-less mutant, freeze fracture (Fig. 4C, D) revealed the presence of 3120 PF particles/μm^2 and 583 EF particles/μm^2. The diameter of the PF particles fell in the range of 5–20 nm with most of the particles falling into the range between 10 and 16 nm. The EF particles were 5–10 nm in diameter. Some rows of particles were evident.

The PSI/PSII-less mutant (Fig. 4E, F) had 2797 PF particles/μm^2 and 251 EF particles/μm^2. On the PF surface the particles were 8–17 nm in diameter. On the EF surface, the particles were 4–20 nm in diameter. No rows of particles were obvious.

4. Discussion

This study was designed to investigate the effect of deletion of PSI on the architecture and structure of the thylakoid membranes in *Synechocystis* sp. PCC 6803. Deletion of PSI leaves only functional PSII as the major photosystem in the membrane and this deletion was found to cause gross morphological changes to the structure and the number of thylakoid membrane sheets in the cell. The lower light conditions in which the cyanobacteria were grown resulted in variations in thylakoid structure compared to WT cells grown in high light conditions. A strain with a deletion of only PSII was not investigated in the present study as Nilsson and coworkers (1992) investigated such a mutant previously using FF and TEM techniques. No difference in the gross morphology of the thylakoid membrane system was observed in the Nilsson et al. study, with the mutants appearing to be similar to wild type cells [22–24].

4.1. Changes in thylakoid architecture caused by low light growth conditions

It is known that the ratio of PSI to PSII is different in thylakoid membranes when cyanobacterial cells are grown in low light as compared to high light [25–27] with the amount of PSI decreasing in low light. In chloroplasts that were investigated after similar treatments, the ultrastructure was modified with an increase in thylakoid membranes and chlorophyll content in low light conditions [28]. The inflated lumens of the wild-type cells grown in low light have been observed before in cyanobacteria grown in periods of dark [29–32] or in aging cells [29]. These inflated lumen were termed “intrathylakoidal vesicles” and described as two thylakoid membranes that are slightly-to-widely separated rather than closely appressed [33]. The cause of the changed appearance has been associated with stress, the change in ratio of PSI to PSII, a reduced plastoquinone pool, or a decrease in chlorophyll content, which was suggested previously for cells aged under optimal light conditions where intrathylakoid vesicle formation was observed [29]. In the present study, the low light conditions represent a variation in environmental conditions that the cyanobacteria have adapted to, possibly causing the change in thylakoid membrane architecture in line with a mechanism or combination of mechanisms cited above. Iron starvation has also been associated with the observation of intrathylakoid vesicles after chlorophyll *a* and PSII reaction centers began to break down [34,35], a similar situation to the mutants investigated here where there is no PSI reaction center. The iron-starved vesiculated cells later showed a complete degradation of the entire thylakoid system, which was also observed in some cells in this study.

The inflated lumen of the low light grown cells from this study allowed the visualization of what appeared to be connections between the thylakoid membrane system and the cytoplasmic membrane at thylakoid membrane convergence sites as has been suspected for many years [10,36–39]. These connections may be more obvious because the inflated thylakoid lumen enhanced the usually small connections. While these cytoplasmic connections were only observed in 7% of cells in this study, it is possible that they may exist in most cells during cell expansion when thylakoid membranes are actively growing, but have been difficult to detect [8,40]. This may be due to the usually small size and transient nature of the connections; characteristics which may maintain the biochemical distinction between the thylakoid and cytoplasmic membranes. This theory is supported by the “hemifusion” model suggested by extensive proteomic analysis of the different membrane fractions from *Synechocystis* [41]. Predicted roles for such connections have included the transport of glycolipids and possibly photosystem precursors to the thylakoid membrane [10,36]. The PratA-D1 PSII precursors have been observed around the periphery of the cell [42,43] and there must be some mechanism for transferring these components to the thylakoid membranes: either via these connections or via lipid bodies [44–46]. At these connections, the lumen appears to be connected to the periplasmic space. This connection may allow transport of

protons from the lumen to the periplasmic space and vice versa. Overall, apart from the inflated lumen, the general cytoplasmic architecture of the low light grown cells was similar to high light grown cells.

4.2. The structure of thylakoid membranes without PSI

Deletion of PSI, leaving PSII as the only functional photosystem, caused the striking formation of tubular thylakoid membranes observed in 74% of the cells examined. Tubular structures were also observed in the PSI/PSII less cells; however, these tubular structures were seen much less frequently (18% of cells) and appeared to have an internal structure distinct from the tubular structures in the PSI-less strain. The change in morphology of the PSI-less mutant may be directly related to the role that PSI has in the membrane structure and be a result of the change in organization and packing of PSII in the membrane. PSII-less mutants, which maintain PSI, show no such tubular structures and appear to have a sheet-like structure similar to that found in WT cells [22–24]. Alternatively, the tubular system may be caused by changes associated with PSI deletion such as an over-reduced plastoquinone pool.

At the higher resolution in the Z-axis provided by electron tomography, an intriguing structure was observed situated below the phycobilisome possibly extending into the lumen of the thylakoid membranes. This is possibly the oxygen evolving complex of PSII that is known to project by 4–5 nm into the lumen from high resolution studies [47,48].

4.2.1. Morphological changes caused by the deletion of PSI and PSII

Surprisingly, deletion of both PSI and PSII from *Synechocystis* sp. PCC 6803 caused little apparent change to thylakoid morphology compared to the high light grown cells except for a decrease in the number of thylakoid membrane pairs and reduced size. The thylakoid membrane pairs were closely appressed and only some smaller and less frequently occurring tubes with different apparent internal and external organization were observed.

4.3. Phycobilisomes

Phycobilisomes are most commonly arranged in orderly rows alternately between two adjacent membranes [49] and this phenotype was obvious in the PSI-less mutant and in the WT cells. The mutant lacking both functional PSI and PSII had phycobilisomes but these were in more disordered arrays, possibly caused by the deletion of the D2 and CP43 proteins of PSII. Some order is still present as seen in the electron tomogram models, which may be due to the membrane anchoring properties of the phycobilisomes themselves. In the low light grown WT cells, the phycobilisomes seemed to be found more often on the peripheral thylakoids, which correlates with the hyperspectral imaging of chlorophylls and phycobilisome pigments [50]. This indicates that there is possibly compartmentalization of the cell and thylakoid membranes in *Synechocystis*. Glycogen granules were also observed between thylakoid membranes with varying electron density similar to that seen in *Cyanothece* sp. ATCC 51142 [51]. Glycogen granules were not observed in the mutant cells possibly because the glycogen was used as a carbon resource due to the limited functionality of photosynthesis in these cell lines.

The prominent phycobilisomes in the PSI-less mutant were expected as phycobilisomes are known to associate with PSII [1,49]. As these are peripheral antenna complexes, it is less likely that they are involved in membrane organization or architecture. The regular arrays of phycobilisomes observed in the PSI-less mutant supports the theory that the phycobilisomes link to PSII forming orderly arrays.

4.4. Freeze fracture particle distribution

Investigations of the particles found on the surface of the thylakoid membranes in all three strains studied showed a number of interesting features; however, the data was not extensive as these cyanobacteria are small and relatively difficult to fracture, particularly the mutant strains as they have reduced numbers of thylakoid membranes. There were differing numbers of EF particles in all three strains with the number of particles in the WT correlating well with the numbers found in other studies in WT cells [22,52]. In a PSII-less strain that lacked the *psbA* gene, D1, D2 and CP47 and so only had functional PSI present, the number of particles on the E-face were approximately half that observed in WT cells [22]. The PSI/PSII-less strain had the least number of particles on the E-face and there seemed to be a large size difference between the particles. This may be due to single molecular complexes such as ATPase or cytochrome oxidase.

The number of PF particles in the low light grown WT cells were smaller than that observed in high light grown cells and this may be a reflection of the changed ratio of PSI:PSII in the thylakoid membranes. Both the mutants also had fewer PF particles than the WT cells. The difference in particle numbers between the two mutant strains was not significant, indicating that the photosystem complexes are maintained in the membrane without the non-functional proteins and this may also explain the variations in size of the particles in the mutant strains. This result was also suggested by Nilsson et al. (1992).

5. Conclusions

The structure of the thylakoid membranes of *Synechocystis* were severely disrupted in the mutant lacking PSI. The change in morphology could be due to the presence of only PSII and the overall charge and structure of the photosystem complexes or to other effects caused by the mutation. There have also been other potential proteins that are not found in the photosynthetic process that may be involved in thylakoid membrane formation including the Vipp1 mutant [53], Alb3 [54], plastoglobulin-like proteins [44] and Slr1768, a SPHF homologue [55]. The roles of these genes are still being elucidated.

Supplementary materials related to this article can be found online at doi:10.1016/j.bbamem.2012.01.019.

Acknowledgements

This research was supported by the U.S. Department of Energy GTL: Genomics Project, #DE-FG03-01ER15251. The electron microscopy and freeze fracture studies were carried out at the Life Sciences Electron Microscopy Facility at Arizona State University. We thank Dr. Doug Chandler for help with interpretation of freeze fracture results and Dan Jenk for scientific editing of the manuscript. Electron tomography was undertaken at the Center for Solid State Sciences, Arizona State University (ASU), Tempe, AZ.

References

[1] R.E. Blankenship, Molecular Mechanisms of Photosynthesis, Blackwell Science Ltd., Malden, 2002.
[2] A. Zouni, H.T. Witt, J. Kern, P. Fromme, N. Krauss, W. Saenger, P. Orth, Crystal structure of photosystem II from *Synechococcus elongatus* at 3.8 angstrom resolution, Nature 409 (2001) 739–743.
[3] W.S. Chow, E.H. Kim, P. Horton, J.M. Anderson, Granal stacking of thylakoid membranes in higher plant chloroplasts: the physicochemical forces at work and the functional consequences that ensue, Photochem. Photobiol. Sci. 4 (2005) 1081–1090.
[4] G.Z. Shen, S. Boussiba, W.F.J. Vermaas, *Synechocystis* sp. PCC 6803 strains lacking Photosystem I and phycobilisome function, Plant Cell 5 (1993) 1853–1863.
[5] S. Ermakova-Gerdes, S. Shestakov, W.F.J. Vermaas, Development of a Photosystem I-less strain of *Synechocystis* sp. PCC 6803 for analysis of mutations in the Photosystem II proteins D2 and CP43, in: P. Mathis (Ed.), Photosynthesis: From Biology to Biosphere, vol. 1, Kluwer, Dordrecht, 1995, pp. 483–486.
[6] T. Kaneko, S. Sato, H. Kotani, A. Tanaka, E. Asamizu, Y. Nakamura, N. Miyajima, M. Hirosawa, M. Sugiura, S. Sasamoto, T. Kimura, T. Hosouchi, A. Matsuno, A. Muraki,

N. Nakazaki, K. Naruo, S. Okumura, S. Shimpo, C. Takeuchi, T. Wada, A. Watanabe, M. Yamada, M. Yasuda, S. Tabata, Sequence analysis of the genome of the unicellular cyanobacterium *Synechocystis* sp. strain PCC 6803. II. Sequence determination of the entire genome and assignment of potential protein-coding regions, DNA Res. 3 (1996) 109–136.
[7] W.F.J. Vermaas, Molecular–genetic approaches to study photosynthetic and respiratory electron transport in thylakoids from cyanobacteria, Biochim. Biophys. Acta, Bioenerg. 1187 (1994) 181–186.
[8] M. Liberton, R.H. Berg, J. Heuser, R. Roth, H.B. Pakrasi, Ultrastructure of the membrane systems in the unicellular cyanobacterium *Synechocystis* sp. strain PCC 6803, Protoplasma 227 (2006) 129–138.
[9] H.E. Mohamed, A.M.L. van de Meene, R.W. Roberson, W. Vermaas, Deletion of *sll1213*, a putative fucose synthetase gene in *Synechocystis* sp. PCC 6803: myxoxanthophyll is required for normal cell wall structure and thylakoid organization in cyanobacteria, J. Bacteriol. 187 (2005) 6883–6892.
[10] A.M.L. van de Meene, M.F. Hohmann-Marriott, W. Vermaas, R.W. Roberson, The three-dimensional structure of the cyanobacterium *Synechocystis* sp. PCC 6803, Arch. Microbiol. 184 (2006) 259–270.
[11] R. Rippka, J. Deruelles, J.B. Waterbury, M. Herdman, R.Y. Stanier, Generic assignments, strain histories and properties of pure cultures of cyanobacteria, J. Gen. Microbiol. 111 (1979) 1–61.
[12] A.R. Spurr, A low-viscosity epoxy resin embedding medium for electron microscopy, J. Ultrastruct. Res. 26 (1969) 31–43.
[13] E.S. Reynolds, Use of lead citrate at high ph as an electron-opaque stain in electron microscopy, J. Cell Biol. 17 (1963) 208-&.
[14] J.C. Russ, R.T. Dehoff, Practical Stereology, 2nd ed. Plenum Press, New York, NY, 2001.
[15] M. Marko, Quantitative techniques in biological TEM, Microsc. Microanal. 10 (Suppl. 2) (2004) 1282–1283.
[16] H. Friedrich, M.R. McCartney, P.R. Buseck, Comparison of intensity distributions in tomograms from BF TEM, ADF STEM, HAADF STEM, and calculated tilt series, Ultramicroscopy 106 (2005) 18–27.
[17] J.R. Kremer, D.N. Mastronarde, J.R. McIntosh, Computer visualization of three-dimensional image data using IMOD, J. Struct. Biol. 116 (1996) 71–76.
[18] D.N. Mastronarde, Dual-axis tomography: an approach with alignment methods that preserve resolution, J. Struct. Biol. 120 (1997) 343–3521.
[19] E.T. O'Toole, M. Winey, J.R. McIntosh, High-voltage electron tomography of spindle pole bodies and early mitotic spindles in the yeast *Saccharomyces cervisiae*, Mol. Biol. Cell 10 (1999) 2017–2031.
[20] C.A. Larabell, D.E. Chandler, The coelomic envelope of *Xenopus laevis* eggs: a quick-freeze, deep-etch analysis, Dev. Biol. 131 (1989) 126–135.
[21] D.D. Kunkel, Thylakoid centers: structures associated with the cyanobacterial photosynthetic membrane system, Arch. Microbiol. 133 (1982) 97–99.
[22] F. Nilsson, D.J. Simpson, C. Jansson, B. Andersson, Ultrastructural and biochemical characterization of a *Synechocystis* 6803 mutant with inactivated *psbA* genes, Arch. Biochem. Biophys. 295 (1992) 340–347.
[23] A.A. Arteni, G. Ajlani, E.J. Boekema, Structural organization of phycobilisomes from *Synechocystis* sp. strain PCC 6803 and their interaction with the membrane. Biochim. Biophys. Acta 1787 (2009) 272–279.
[24] J. Barber, E.P. Morris, P.C.A. da Fonseca, Interaction of the allophycocyanin core complex with photosystem II, Photochem. Photobiol. Sci. 2 (2003) 536–541.
[25] A. Murakami, S.J. Kim, Y. Fujita, Changes in photosystem stoichiometry in response to environmental conditions for cell growth observed with the cyanophyte *Synechocystis* PCC 6714, Plant Cell Physiol. 38 (1997) 392–397.
[26] A. Murakami, Y. Fujita, Regulation of stoichiometry between PSI and PSII in response to light regime for photosynthesis observed with *Synechocystis* PCC 6714: relationship between redox state of Cyt b_6f complex and regulation of PSI formation, Plant Cell Physiol. 34 (1993) 1175–1180.
[27] A. Manodori, A. Melis, Cyanobacterial acclimation of Photosystem I or Photosystem II light, Plant Physiol. 82 (1986) 185–189.
[28] A. Melis, Light regulation of photosynthetic membrane structure, organization, and function, J. Cell. Biochem. 24 (1984) 271–285.
[29] L.R. Ermakova, K.A. Nikitina, M.V. Gusev, Age-related changed in the ultrastructure of *Anabaena variabilis* cells, Mikrobiologiia 46 (1977) 324–328.
[30] O.I. Baulina, M.V. Gusev, Dynamics of ultrastructural changes in the obligately phototrophic alga *Anabaena variabilis* during preservation of viability in the dark, Sov. Plant Physiol. 25 (1978) 922–926.
[31] K.A. Nikitina, L.V. Bogorov, M.V. Gusev, The cellular ultrastructure of obligate phototrophic blue green alga *Anabaena variabilis* in cultures dying in the dark, Mikrobiologiia 43 (1974) 1079–1083.
[32] O.I. Baulina, T.G. Korzhenevskaya, M.V. Gusev, Electron microscopic investigation of dark and photooxidative degradation of the blue green alga *Anabaena variabilis*, Mikrobiologiia 46 (1977) 128–133.
[33] J.F. Stolz, Structure of Phototrophic Prokaryotes, CRC Press, Boca Raton, 1991, p. 131.
[34] L.P. Hardie, D.L. Balkwill, S.E. Stevens, Effects of iron starvation on the physiology of the cyanobacterium *Agmenellum quadruplicatum*, Appl. Environ. Microbiol. 45 (1983) 999–1006.
[35] L.P. Hardie, D.L. Balkwill, S.E. Stevens, Effects of iron starvation on the ultrastructure of the cyanobacterium *Agmenellum quadruplicatum*, Appl. Environ. Microbiol. 45 (1983) 1007–1017.
[36] S.A. Nierzwicki-Bauer, D.L. Balkwill, S.E. Stevens, 3-dimensional ultrastructure of a unicellular cyanobacterium, J. Cell Biol. 97 (1983) 713–722.
[37] S.A. Nierzwicki-Bauer, D.L. Balkwill, S.E. Stevens, The use of high-voltage electron microscopy and semi-thick sections for examination of cyanobacterial thylakoid membrane arrangements, J. Microsc. Oxf. 133 (1984) 55–60.
[38] B.V. Gromov, K.A. Mamkaeva, Connection of thylakoids with plasmalemma in cyanobacteria of genus *Synechococcus*, Microbiology 45 (1976) 790–791.
[39] M.M. Allen, Photosynthetic membrane system in *Anacystis nidulans*, J. Bacteriol. 96 (1968) 836–841.
[40] D. Schneider, E. Fuhrmann, I. Scholz, W.R. Hess, P.L. Graumann, Fluorescence staining of live cyanobacterial cells suggest non-stringent chromosome segregation and absence of a connection between cytoplasmic and thylakoid membranes, BMC Cell Biol. 8 (2007) 39.
[41] T. Pisareva, J. Kwon, J. Oh, S. Kim, C. Ge, A. Wieslander, J.-S. Choi, B. Norling, Model for membrane organization and protein sorting in the cyanobacterium Synechocystis sp PCC 6803 inferred from proteomics and multivariate sequence analyses, J. Proteome Res. 10 (2011) 3617–3631.
[42] B. Rengstl, U. Oster, A. Stengel, J. Nickelsen, An intermediate membrane subfraction in cyanobacteria is involved in an assembly network for photosystem II biogenesis, J. Biol. Chem. 286 (2011) 21944–21951.
[43] M. Schottkowski, S. Gkalympoudis, N. Tzekova, C. Stelljes, D. Schuenemann, E. Ankele, J. Nickelsen, Interaction of the periplasmic PratA factor and the PsbA (D1) protein during biogenesis of photosystem II in Synechocystis sp PCC 6803, J. Biol. Chem. 284 (2009) 1813–1819.
[44] F.X. Cunningham, A.B. Tice, C. Pham, E. Gantt, Inactivation of genes encoding plastoglobulin-like proteins in *Synechocystis* sp. PCC 6803 leads to a light-sensitive phenotype. J. Bacteriol. 192 (2010) 1700–1709.
[45] F. Kessler, P.-A. Vidi, Plastoglobule lipid bodies: their functions in chloroplasts and their potential for applications, Adv. Biochem. Eng. Biotechnol. 107 (2007) 153–172.
[46] J. Nickelsen, B. Rengstl, A. Stengel, M. Schottkowski, J. Soll, E. Ankele, Biogenesis of the cyanobacterial thylakoid membrane system — an update, FEMS Microbiol. Lett. 315 (2010) 1–5.
[47] A. Guskov, J. Kern, A. Gabdulkhakov, M. Broser, A. Zouni, W. Saenger, Cyanobacterial photosystem II at 2.9-angstrom resolution and the role of quinones, lipids, channels and chloride, Nat. Struct. Mol. Biol. 16 (2009) 334–342.
[48] Y. Umena, K. Kawakami, J.-R. Shen, N. Kamiya, Crystal structure of oxygen-evolving photosystem II at a resolution of 1.9 angstrom, Nature 473 (2011) 55–60.
[49] J. Olive, G. Ajlani, C. Astier, M. Recouvreur, C. Vernotte, Ultrastructure and light adaptation of phycobilisome mutants of *Synechocystis* PCC 6803, Biochim. Biophys. Acta 1319 (1997) 275–282.
[50] W. Vermaas, J.A. Timlin, H.D.T. Jones, M.B. Sinclair, L.T. Nieman, S.W. Hamad, D.K. Melgaard, D.M. Haaland, *In vivo* hyperspectral confocal fluorescence imaging to determine pigment localization and distribution in cyanobacterial cells, PNAS 105 (2008) 4050–4055.
[51] M. Liberton, J.R. Austin, R.H. Berg, H.B. Pakrasi, Unique thylakoid membrane architecture of a unicellular N-2-fixing cyanobacterium revealed by electron tomography, Plant Phys. 155 (2011) 1656–1666.
[52] T.H. Giddings, Membrane architecture of oxygen-evolving photosynthetic prokaryotes, Department of Molecular, Cellular and Developmental Biology, University of Colorado, Boulder, 1979, p. 155.
[53] E. Fuhrmann, S. Gathmann, E. Rupprecht, J.R. Golecki, D. Schneider, Thylakoid membrane reduction affects the photosystem stoichiometry in the cyanobacterium *Synechocystis* sp. PCC 6803, Plant Physiol. 149 (2010) 735–744.
[54] E. Spence, S. Bailey, A. Nenninger, S.G. Moller, C. Robinson, A homolog of Albino3/OxaI is essential for thylakoid biogenesis in the cyanobacterium Synechocystis sp PCC6803, J. Biol. Chem. 279 (2004) 55792–55800.
[55] S.J. Bryan, N.J. Burroughs, C. Evered, J. Sacharz, A. Nenninger, C.W. Mullineaux, E.M. Spence, Loss of the SPHF homologue Slr1768 leads to a catastrophic failure in the maintenance of thylakoid membranes in Synechocystis sp PCC 6803, PLoS One 6 (2011).